Manganese and Cobalt in the Nonheme Metal-binding Site of a Biosynthetic Model of Heme-Copper Oxidase Superfamily Confer Oxidase Activity through Redox-inactive Mechanism

Julian H. Reed,[1] Yelu Shi,[2] Qianhong Zhu,[3] Saumen Chakraborty,[4] Evan N. Mirts,[5] Igor D. Petrik,[6] Ambika Bhagi-Damodaran,[7] Matthew Ross,[8] Pierre Moënne-Loccoz,[3]* Yong Zhang,[2]* and Yi Lu[1,5,6]*

1 Department of Biochemistry, University of Illinois at Urbana-Champaign, Urbana, IL, 61801, USA

2 Department of Biomedical Engineering, Chemistry, and Biological Sciences, Stevens Institute of Technology, Hoboken, NJ, 07030, USA

3 Division of Environmental & Biomolecular Systems, Institute of Environmental Health, Oregon Health & Science University, Portland, OR, 97239, USA

4 Department of Chemistry & Biochemistry, University of Mississippi, Oxford, Mississippi, 38677, USA

5 Center for Biophysics and Quantitative Biology, University of Illinois at Urbana-Champaign, Urbana, IL, 61801, USA

6 Department of Chemistry, University of Illinois at Urbana-Champaign, Urbana, IL, 61801, USA

7 Department of Pharmaceutical Chemistry, University of California, San Francisco, San Francisco, CA, 94143, USA

8 Department of Chemistry, Northwestern University, Evanston, IL, 60208, USA

* Corresponding authors, email: yi-lu@illinois.edu; yong.zhang@stevens.edu; moennelo@ohsu.edu

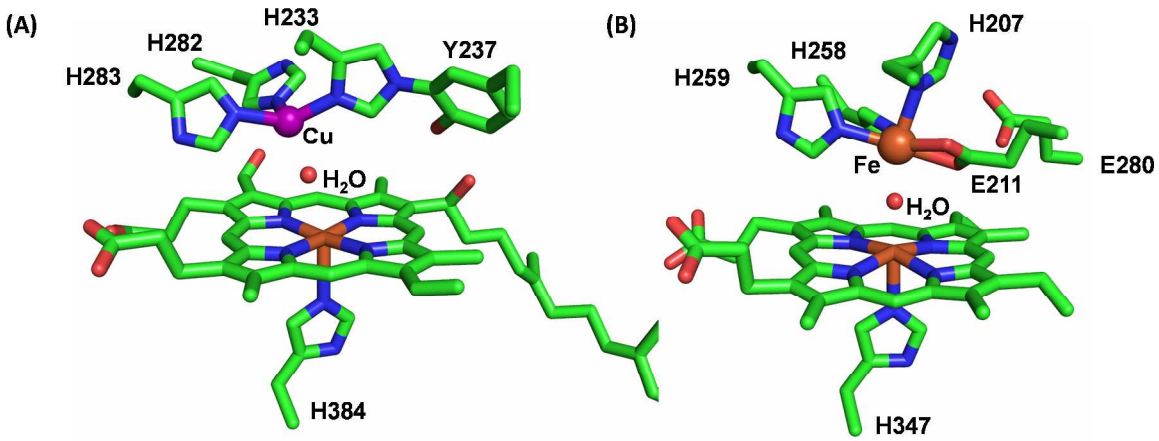

Figure S1. Crystal structures of (A) ba3 oxidase (PDB code 1XME) and (B) cNOR (PDB code 3O0R). Water molecules are shown as small red spheres, while nonheme metal ions are depicted as large purple and red spheres for copper and iron, respectively.

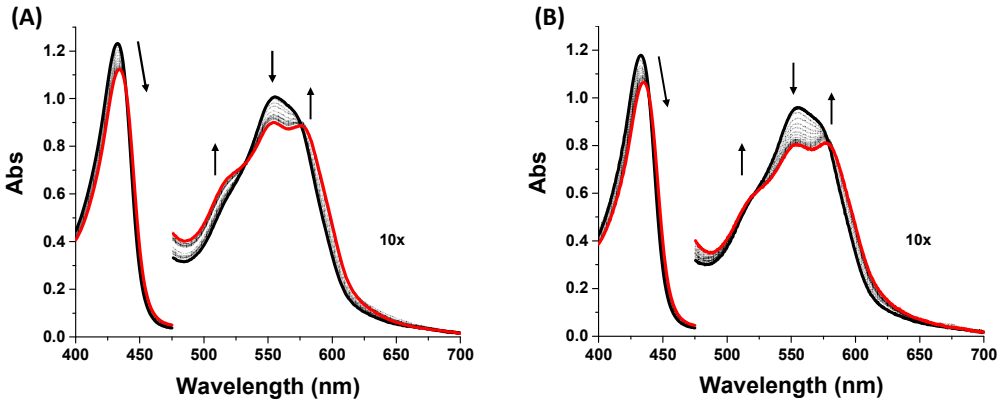

Figure S2. Nonheme metal titrations to Fe_BMb using (A) $MnCl_2$ and (B) $CoCl_2$. Arrows represent the change in spectra upon addition of nonheme metal, with starting spectrum (black), transitioning to the final spectrum (red). Molar equivalents of nonheme metal used were: 0.2, 0.4, 0.6, 0.8, 1, 1.5, 2, 2.5, 3, 4, and 5. The proteins were in a buffer solution of 50 mM Bis Tris pH 7.

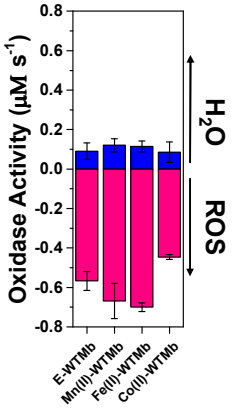

Figure S3. Oxidase activity of 18 μM WTMb in 100 mM potassium phosphate buffer pH 6 with 250 μM O_2, 1.8 mM TMPD, 18 mM ascorbate, and different nonheme metals added. The measured rates of O_2 reduction forming either water (blue) or ROS (red) are shown. Error bars indicate standard deviation.

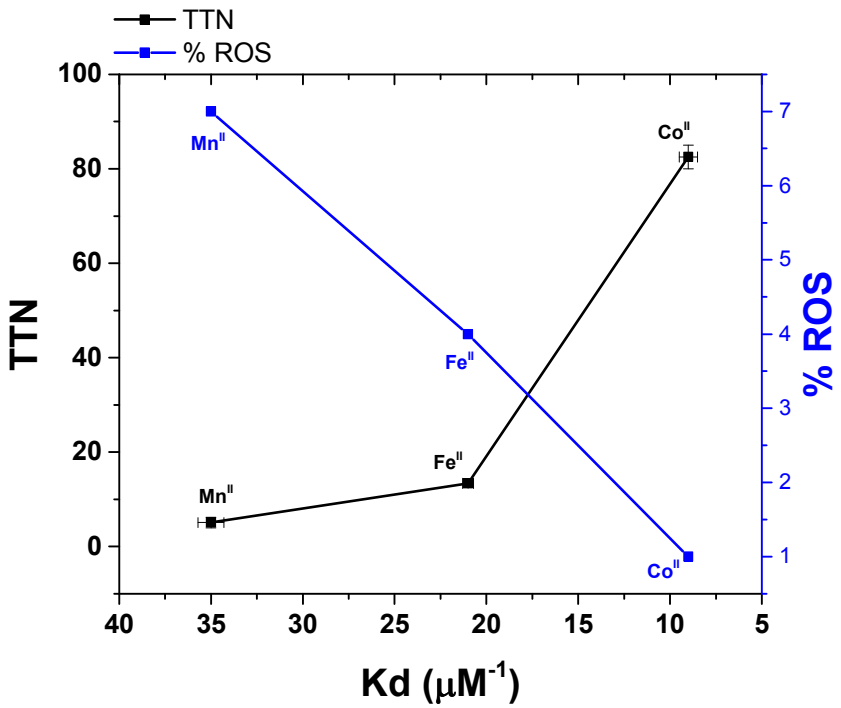

Figure S4. Comparison of TTN and % ROS formation at 18 μM protein during O_2 reduction to the dissociation constant (K_d) for each nonheme metal variant of $Fe_BMb(Fe^{II})$. Each data point is labeled with its corresponding nonheme metal.

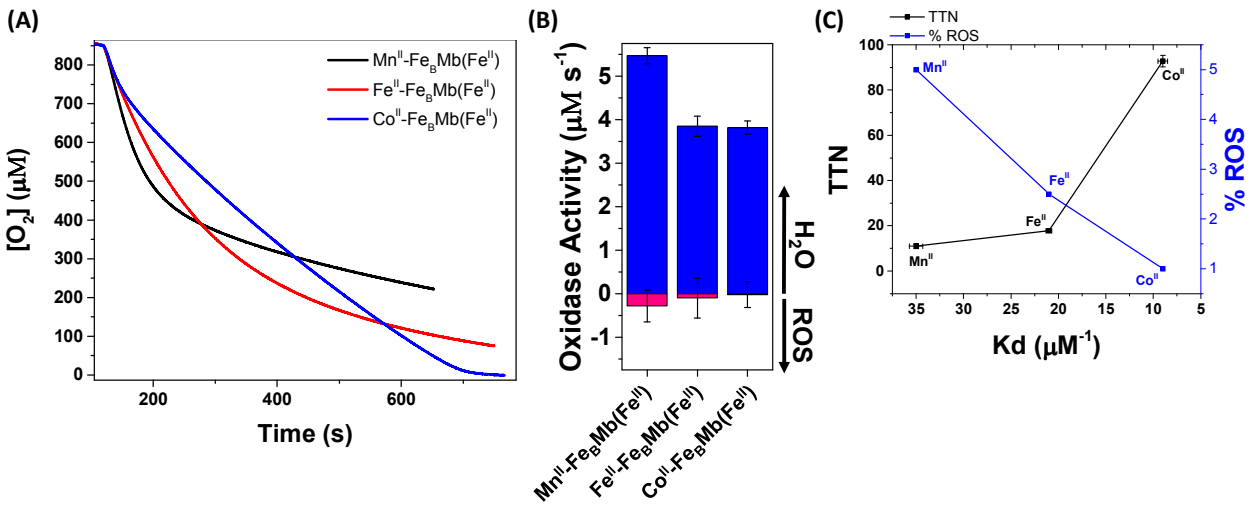

Figure S5. (A) O_2 consumption traces of Mn^{II}-$Fe_BMb(Fe^{II})$ (black), Fe^{II}-$Fe_BMb(Fe^{II})$ (red), and Co^{II}-$Fe_BMb(Fe^{II})$ (blue) carried out using 40 μM protein. (B) O_2 consumption rates for the three protein variants. (C) Comparison of TTN and % ROS formation at 40 μM protein during O_2 reduction to the dissociation constant (K_d) for each nonheme metal variant of $Fe_BMb(Fe^{II})$. Each data point is labeled with its corresponding nonheme metal.

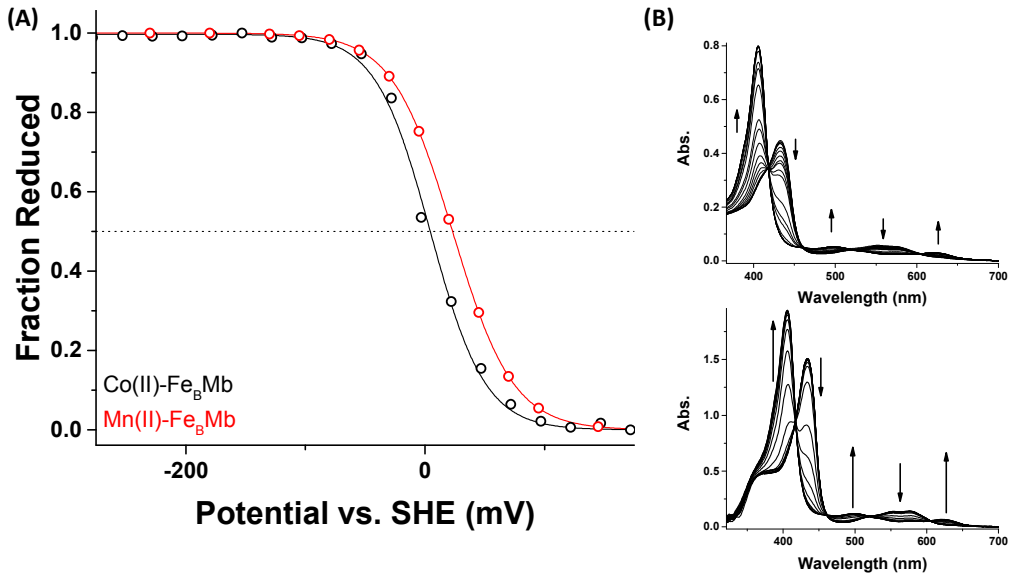

Figure S6. (A) Nernst fit of the spectroelectrochemical plot for Mn^{II}- and Co^{II}-Fe_BMb(Fe^{II}). The center dotted line indicates the point at which the fraction of reduced and oxidized protein is equal, and corresponds to the heme redox potential. (B) Spectroelectrochemical measurements of the Fe_BMb heme reduction potential with Mn^{II} (top) and Co^{II} bottom bound at the nonheme site.

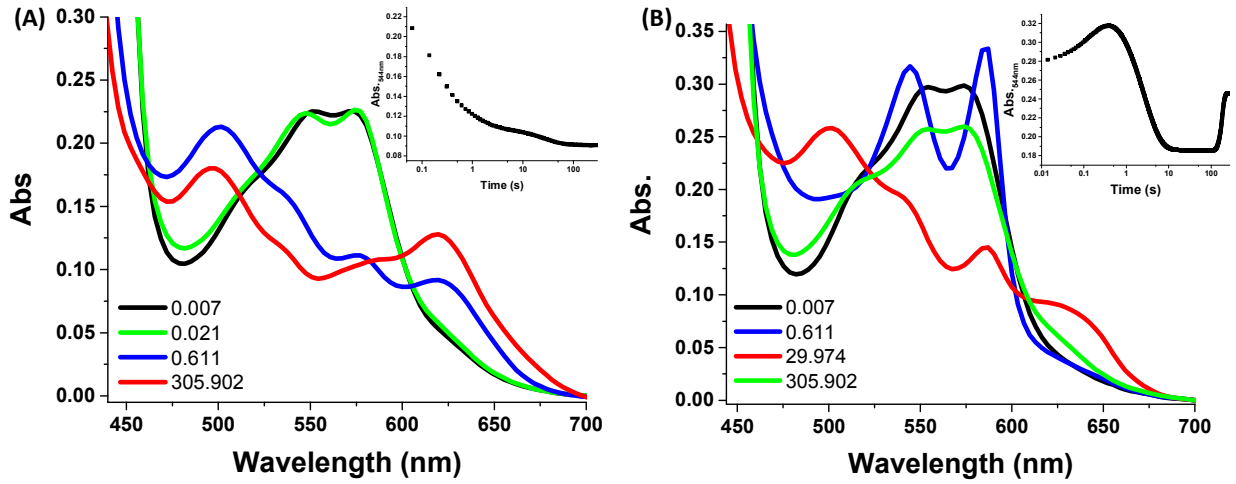

Figure S7. Stopped-flow UV/Vis spectra of the reaction of ~50 µM (A) Mn^{II}- and (B) Co^{II}-Fe_BMb(Fe^{II}) mixed with O_2-saturated 100 mM potassium phosphate pH 6 in the presence of 5 mM/50 mM TMPD/ascorbate. The insets show a time trace at 544 nm.

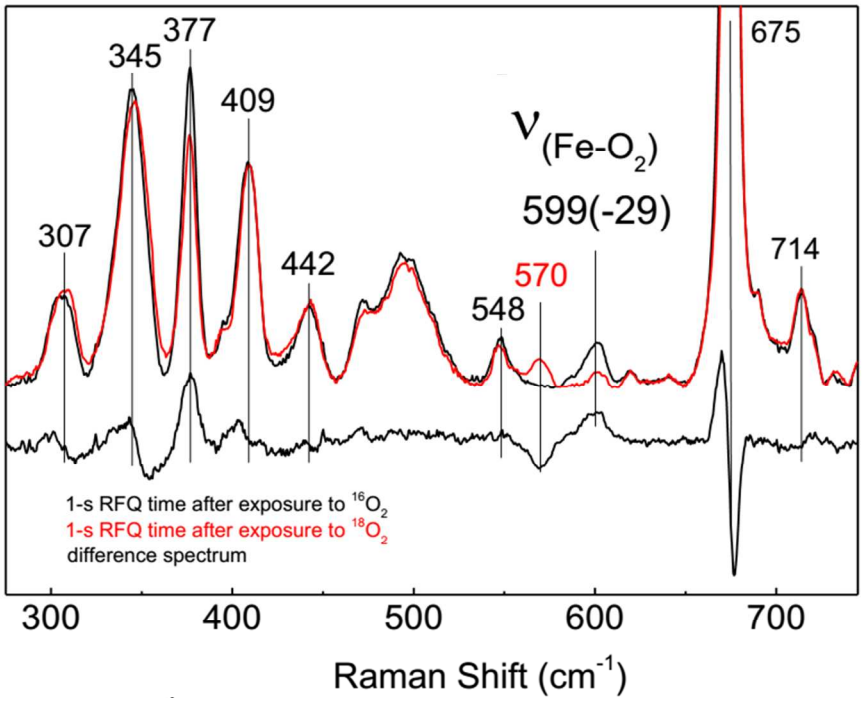

Figure S8. Low-frequency RR spectra of Co^{II}-FeBMb(Fe^{II}-O_2) prepared similarly to as described for Figure 5, and collected at 407 nm excitation.

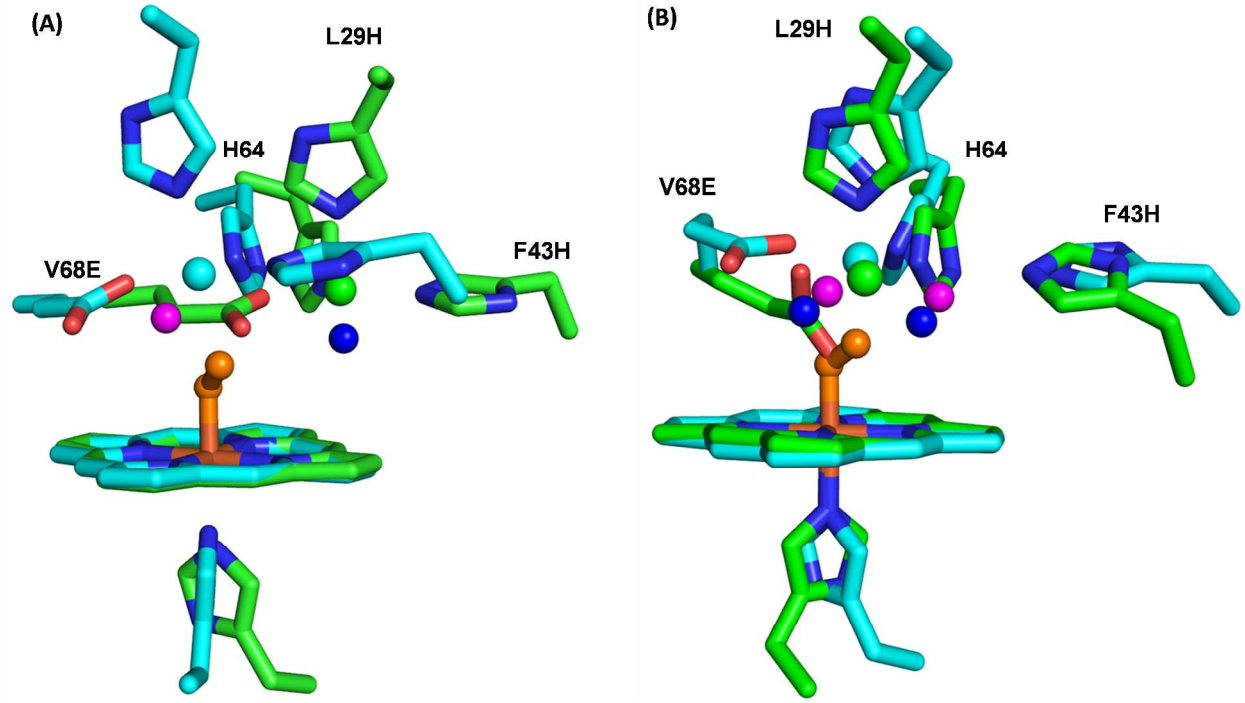

Figure S9. Structural overlay of energy optimized active site structures of (A) Mn^{II}- and (B) Co^{II}-$Fe_BMb(Fe^{II})$ before and after addition of O_2. In (A) Mn^{II}-$Fe_BMb(Fe^{II})$ is represented as green and cyan sticks before and after addition of O_2, respectively. Mn^{II} is shown as a green or cyan sphere before and after addition of O_2, respectively. Water molecules are shown as blue and magenta spheres, before and after addition of O_2, respectively. Heme-bound O_2 is displayed as orange spheres. Main chain and other atoms are not shown for clarity. The same color scheme is used for (B).

Table S1: Diffraction and refinement data for Mn^{II}- and Co^{II}-Fe_BMb(Fe^{II})

	Mn^{II}-Fe_BMb(Fe^{II})	Co^{II}-Fe_BMb(Fe^{II})
Data Collection		
Source	SSRL Beamline BL14-1	SSRL Beamline BL14-1
Date	2016-07-20	2015-06-11
Detector	CCD, Rayonix MX325HE	CCD, Rayonix MX325HE
Wavelength (Å)	1.2	1.2
Data Reduction		
Software	HKL2000	HKL2000
Spacegroup	$P2_12_12_1$	$P2_12_12_1$
Unit cell (a x b x c; Å)	39.785 x 48.422 x 78.45	39.66 x 47.33 x 76.06
Resolution range (highest shell)	50 – 1.58	35.16 – 2.00
Unique reflections	21305	14401
Completeness (%)	99.2	99.3
Redundancy	4.7	4.2
$\langle I/\sigma(I) \rangle$	55.85	19.36
Refinement	PHENIX	PHENIX
Resolution range (highest shell)	39.225 – 1.5799	35.164 – 1.995
Reflections	21252	14401
Completeness (%)	99.7	76.65
R_{work}	0.2226	0.1941
R_{free}	0.2519	0.2444
Molecules in ASU	1	1
RMSD Bonds (Å)	0.006	0.007
RMSD Angles (°)	0.902	1.554

Computational results

1. Resting state:

For Co^{II}-Fe_BMb(Fe^{II}), the initial setup of electronic configuration is that Co(II) is in high spin (S = 3/2) based on the high spin feature of several metal systems with this non-heme site,[1] and Fe(II) is in low spin (S = 0) based on its six-coordination. The x-ray and the optimized structures for the active site are shown in Figure C1. In the x-ray structure of Co^{II}-Fe_BMb(Fe^{II}), Co has a trigonal bipyramidal five-coordinate structure: one with Glu68, two with His29 and His64, and the other two with W39 and W40. W39 forms a hydrogen bond with His43. Glu68 also coordinates with Fe, which is clearly different from the case for Mn where Glu68 does not coordinate with Fe. These structural features are maintained in the optimized structure (see Figure C1), which further supports the x-ray structural finding.

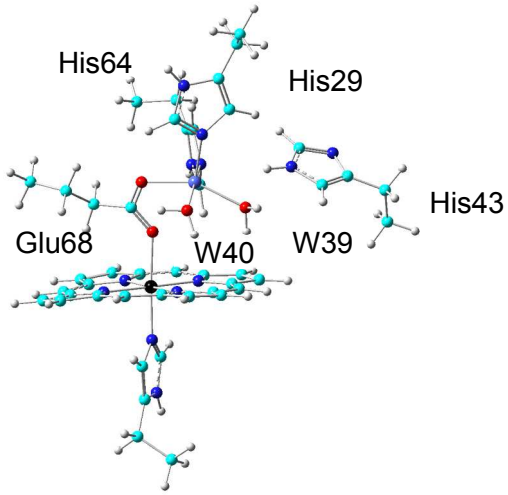

Figure C1. Optimized active site structure of Co^{II}-Fe_BMb(Fe^{II}).

For Mn^{II}-Fe_BMb(Fe^{II}), the initial setup of electronic configuration is similar that Mn(II) is in high spin (S = 5/2) based on the high spin feature of several metal systems with this non-heme site,[1] and Fe(II) is in high spin (S = 2) based on five-coordinate deoxymyoglobin spin state. The x-ray and the optimized structures for the active site are shown in Figure C2. In the x-ray structure of Mn^{II}-Fe_BMb(Fe^{II}), Mn has a trigonal bipyramidal five coordinating structure, coordinating with Glu68, His29, His43, His64, and W1. However, different from Co^{II}-Fe_BMb(Fe^{II}), Glu68 does not coordinate with Fe here. These structural features are also maintained in the optimized structure (see Figure C2), which again supports the x-ray structural finding.

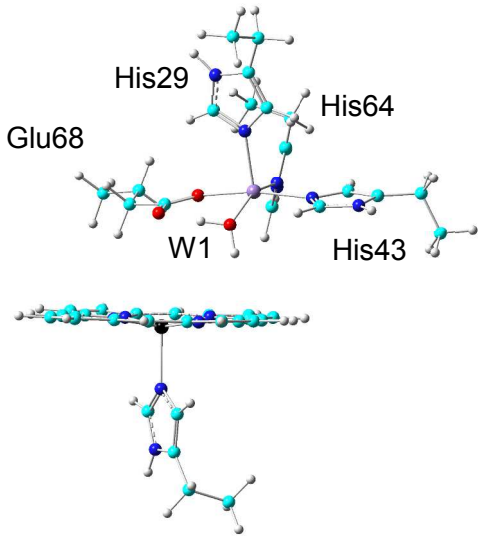

Figure C2. Optimized active site structure of Mn^{II}-Fe_BMb(Fe^{II}).

2. O_2 bound state:

When O_2 is bonded to both Fe and Co, four different initial electronic configurations were examined, with low spin Fe(III) ferromagnetically and antiferromagnetically coupled to high spin Co(II) or Co(III) respectively, and Fe always anti-ferromagnetic coupled to the O_2 moiety. [1-3] However, after geometry optimization, all calculations converged to have only Co(II) based on spin densities of ~2.8 e indicating S = 3/2, and thus only two distinctive structures as shown in Figure C3. This is consistent with experiment that Co is not oxidized. In addition, compared with the current method B3LYP which has 18% Hartree-Fock exchange, we examined the results of using two additional functionals, BHandHLYP and BPW91 with 50% and 0% Hartree-Fock exchange respectively. Even with an initial setup as Co(III) for the oxy-bound form, after geometry optimization, in the final results, Co's spin densities of 2.872 e and 2.786 e clearly indicates that it is still Co(II) (S=3/2), and thus supports the conclusion of non-oxidized Co(II) by the B3LYP method. The structural results show that when O_2 is added to the system, the coordination bond between Fe and Glu68 is broken, and O_2 is coordinated to both Co and Fe. So Co now has an octahedral six-coordination. The O atom in O_2 coordinated to Fe is named as Ob and the other one is named as Ot. The Gibbs free energy difference of Co(II)-Fe_BMb-O_2^--F (F for ferromagnetic coupling) and Co(II)-Fe_BMb-O_2^--AF (AF for antiferromagnetic coupling) is < 1 kcal/mol. Hence, we will focus on Co(II)-Fe_BMb-O_2^--AF in the following studies. In this case, the O-O bond is elongated by 0.026 Å compared to the empty non-heme metal system,[1] indicating that Co(II) indeed helps activate O_2 moiety

as found experimentally. This O_2 bound state was found to be thermodynamically stable compared to the resting state with a Gibbs free energy change of -15.71 kcal/mol.

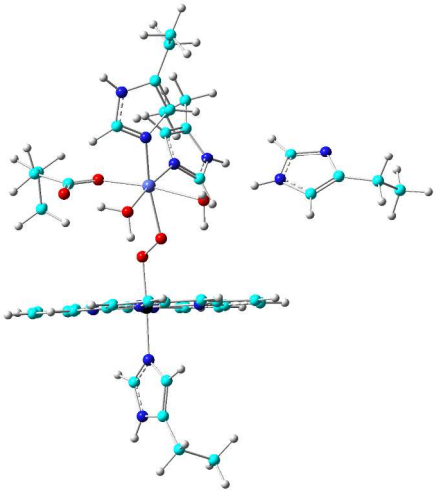

Co(II)-Fe_BMb-O_2^--F

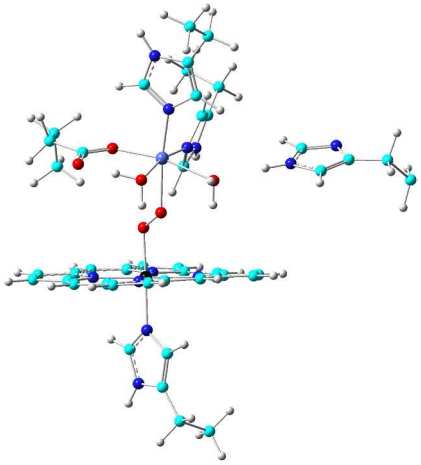

Co(II)-Fe_BMb-O_2^--AF

Figure C3. Optimized structures of four guesses of Co-Fe_BMb-O_2

For Co system, the schematic electronic configuration of metal 3d orbital/O_2 π interactions is shown below. In addition, as shown in the frontier MO picture below (αHOMO-3, isosurface contour value=±0.02 au), there is clear bonding interaction between Fe dπ and O_2 π* due to electron transfer from Fe^{II} to O_2 to form the anti-ferromagnetically coupled Fe^{III} and O_2^-. In contrast, there is no such interaction between Co and O_2 as shown in the same picture.

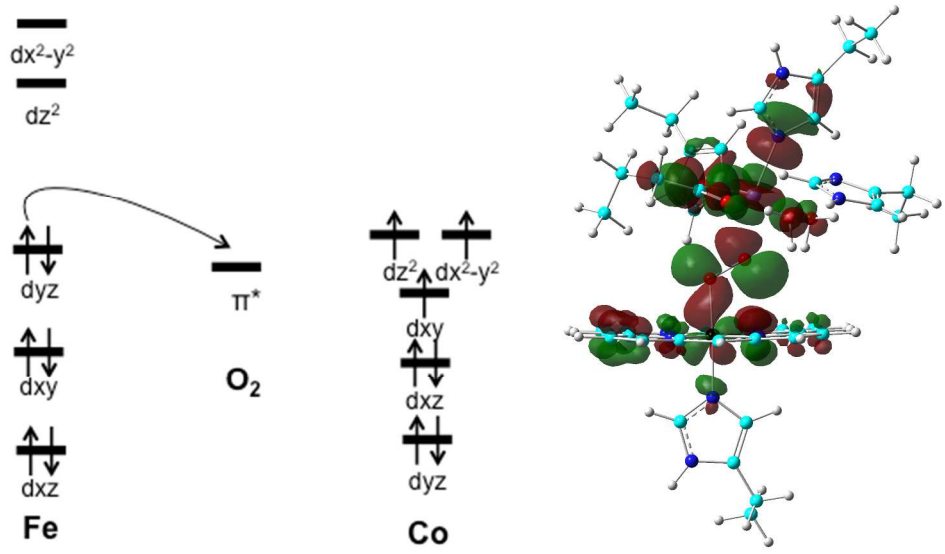

Figure C4. Electronic configuration and orbital plots of metal 3d orbital/O_2 π interactions.

After O_2 binding, the more centrosymmetric Co(II) site can be seen by the following two changes. First, the coordination number changes from five to six. Second, as shown in the following table, the significantly changed angles (those in red) all become closer to 90 or 180 degrees: the N_{E68}-Co-O_{W3} angle is 15° closer to 180°, and N_{H29}-Co-O_{W3}, N_{H64}-Co-O_{W3}, N_{E68}-Co-O_{W40} angles have ca. 4-11° closer to 90°. All other angle changes are smaller than 2 degrees. Such structural changes support the more centrosymmetric feature.

Ligand-Co-Ligand angles in optimized Co-Fe_BMb and Co-Fe_BMb-O_2 models

	N_{H29}-Co-N_{H64}	N_{H29}-Co-N_{E68}	N_{H29}-Co-O_{W3}	N_{H29}-Co-O_{W40}
Co(II)-Fe_BMb	99.8	97.3	104.3	89.9
Co(II)-FeBMb-O_2^--AF	99.4	95.6	93.1	89.8
	N_{H64}-Co-N_{E68}	N_{H64}-Co-O_{W3}	N_{H64}-Co-O_{W40}	
Co(II)-Fe_BMb	96.0	95.7	170.4	
Co(II)-FeBMb-O_2^--AF	95.4	91.3	168.1	
	N_{E68}-Co-O_{W3}	N_{E68}-Co-O_{W40}	O_{W3}-Co-O_{W40}	
Co(II)-Fe_BMb	153.3	82.4	82.1	
Co(II)-FeBMb-O_2^--AF	168.0	91.2	80.6	

Same to the case for Co, when O_2 is bonded to both Fe and Mn, four different initial electronic configurations were examined, with low spin Fe(III) ferromagnetically and antiferromagnetically coupled to high spin Mn(II) or Mn(III) respectively, and Fe always anti-ferromagnetic coupled to the O_2 moiety.[1-3] However, after geometry optimization, three distinctive structures were obtained as shown in Figure C5.

For the two initial Mn(II) structure, only Mn(II)-Fe_BMb-O_2^--AF is stable with Mn spin density of 4.812 e (S=5/2), while the Mn(II)-Fe_BMb-O_2^--F setup results in the oxidized Mn(III)-Fe_BMb-O_2^{2-}-F with Mn spin density of 4.057 e (S=2). The two Mn(III) structures finished the same as initial configurations with Mn spin density of ~4.0 e (S=2). However, the Mn(II)-Fe_BMb-O_2^--AF state is of lower Gibbs free energy than the two Mn(III) states by 4.52 (ferromagnetically coupled metals) and 4.72 kcal/mol (anti-ferromagnetically coupled metals). So, in the case of Mn, it is also not oxidized upon O_2 binding, consistent with experiment. In this case, the O-O bond is elongated by 0.024 Å compared to the empty non-heme metal system,[1] indicating that Mn(II) also helps activate O_2 for reaction as found experimentally. This O_2 bound state was found to be thermodynamically stable compared to the resting state with a Gibbs free energy change of -1.43 kcal/mol. So, the heme-oxy intermediate in the case of Co is more stable than that with Mn.

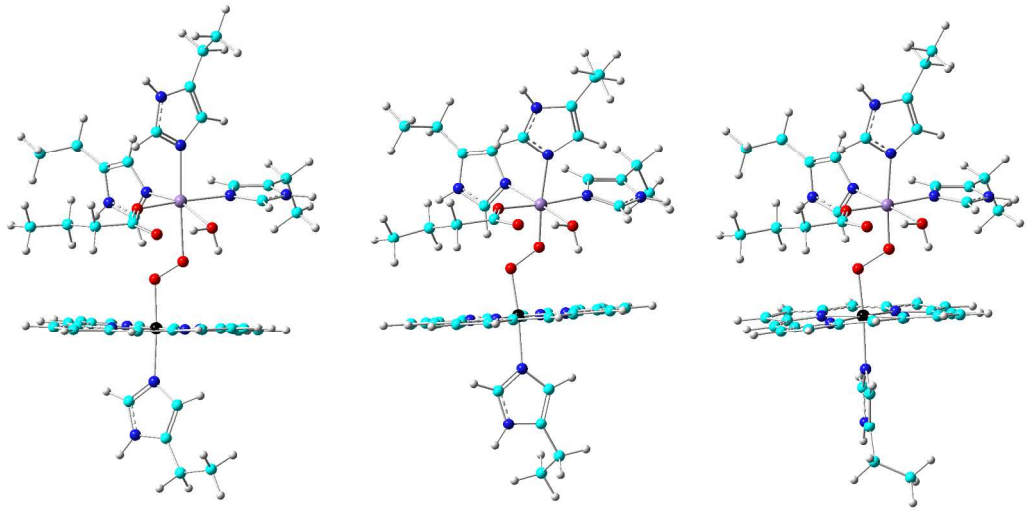

Mn(II)-Fe_BMb-O_2^--AF Mn(III)-Fe_BMb-O_2^{2-}-F Mn(III)-Fe_BMb-O_2^{2-}-AF

Figure C5. Optimized structures of Mn-Fe_BMb-O_2

By using a special computational technique in Gaussian 09, i.e., the constraint C α atoms are frozen but not fixed, the subsequent frequency calculation following the geometry optimization does not have negative/imaginary values.

For the O_2 binding, as shown below, electronic energies (ΔE's), zero-point energy corrected electronic energies (ΔE_{ZPE}'s), enthalpies (ΔH's), and free energies (ΔG's) all give the same trend: Co system is more stable than Mn.

Energy change of O_2 binding

	ΔE kcal/mol	ΔE_{ZPE} kcal/mol	ΔH kcal/mol	ΔG kcal/mol
Co(II)-Fe_BMb	0.00	0.00	0.00	0.00

Co(II)-Fe_BMb-O_2^--AF	-25.11	-23.89	-24.13	-15.71
Mn(II)-Fe_BMb	0.00	0.00	0.00	0.00
Mn(II)-Fe_BMb-O_2^--AF	-17.80	-13.69	-14.71	-1.43

References of Computational Section

1. Bhagi-Damodaran, A.; Michael, M. A.; Zhu, Q. H.; Reed, J.; Sandoval, B. A.; Moënne-Loccoz, P.; Zhang, Y.; Lu, Y. *Nature Chem.* **2017**, *9*, 257-263.
2. Ling, Y.; Zhang, Y. Deciphering Structural Fingerprints for Metalloproteins with Quantum Chemical Calculations. In *Annual Reports in Computational Chemistry*; Wheeler, R. A., Ed. Elsevier: New York, 2010; Vol. 6, pp 65-77.
3. Chen, H.; Ikeda-Saito, M.; Shaik, S. *J. Am. Chem. Soc.* **2008**, *130*, 14778-14790.